Pramāṇa – J. Phys., Vol. 28, No. 4, April 1987, pp. 415–424. © Printed in India.

Precession photography of fibres: Prediction of patterns

M SUNDARAMOORTHY
Molecular Biophysics Unit, Indian Institute of Science, Bangalore 560 012, India

MS received 21 November 1986; revised 25 February 1987

Abstract. The Buerger precession method of recording x-ray diffraction patterns can also be used for fibres. This method has some advantages over the conventional flat plate method. Since the fibre has inherent cylindrical symmetry, the precession photograph of the fibre is equivalent to the 'rotation-precession' photograph of a single crystal. An analytical prediction of diffraction patterns of the rotation-precession photography is discussed. Also, experimental data are provided to confirm the validity of the equations derived.

Keywords. Fibre; diffraction; precession method; pattern prediction.

PACS No. 61·10

1. Introduction

X-ray diffraction patterns of fibres are generally recorded with flat plate cameras. Occasionally, necessity arises to record the meridional and near meridional reflections in the investigation of fibres. In such instances, fibres are tilted, with respect to the x-ray beam through a particular angle corresponding to the layer of interest. The major disadvantage of this method is that it requires recording of as many photographs as the number of layers and also prior knowledge of the period of repeat along the fibre axis for the calculation of tilt angles. Howsman and Walter (1960) had suggested the application of the well-known Buerger precession method which permits meridional and near-meridional reflections to be recorded on a single photograph. In addition, the precession method results in an undistorted image of the reciprocal lattice (RL). King (1966) analyzed the imaging geometry and related the resolution to the layer line screen parameters and the precession angle. He had developed a graphical method of visualizing the images using the geometrical construction of Buerger (1964). This article presents an analytical approach to constructing diffraction images produced by fibres in the precession geometry. The analysis presented here was developed from an earlier study on the "rotation-precession method" using single crystals (Sundaramoorthy *et al* 1986).

2. Diffraction geometry

The RL of a uniaxial fibre is cylindrically symmetrical about the fibre axis. In other words, the RL of a fibre is made up of rings coaxial with the fibre axis. On the other hand, for a single crystal the RL is made up of discrete points. However, single crystal x-ray diffraction might mimic fibre diffraction on rotating the crystal about a chosen axis. Similarly, precession picture recorded for a fibre is equivalent to a rotation-

precession photograph of the single crystal. In this paper, we derive analytical expressions describing the image of a rotation-precession or an equivalent fibre precession photograph. We also provide experimental results demonstrating the validity of the derivation and the usefulness of the method.

The normal Buerger precession camera can be used to record the rotation-precession photograph, by additionally allowing the drum to rotate at a speed unrelated to that of the precession motion. The geometry of the experimental set-up is such that: (i) the crystal tilts with respect to the x-ray beam and also it rotates about the spindle axis; (ii) the film precesses about the x-ray beam.

3. Analysis of the rotation-precession method

The precession motion of the film may be decomposed into two tilt components, (a) μ_r about the rotation axis and (b) μ_t, parallel to the rotation axis. When the crystal is exactly perpendicular to the x-ray beam, μ_r is maximum (μ_0), and μ_t is zero. On the other hand, when the crystal is maximally tilted, the film tilt μ_t is also maximum (μ_0) and μ_r is zero. The orientation of the film, during its precession, is decomposed as mentioned, with $\mu_r = \mu_0 \cos\theta$ and $\mu_t = \mu_0 \sin\theta$, where θ is the angle described by the radius vector on the base of the precession cone (The zero of this angle is defined as the position of maximum tilt of the film about the rotation axis.).

The relationships between film coordinates (x, y) and RL coordinates (ξ, ζ) are derived in four steps of increasing complexity:

(a) Crystal and film normal to the x-ray beam.

(b) Crystal perpendicular to the x-ray beam and film tilted by μ_r about the rotation axis.

(c) Crystal and film tilted by μ_t with respect to the x-ray beam.

(d) Crystal and film tilted by μ_t with respect to the x-ray beam and film tilted by μ_r about the rotation axis.

We shall assume that the crystal is continuously rotating about the mounted axis.

4. Crystal and film normal to the x-ray beam

This is the normal rotation photography used for single crystals. The expressions relating (x, y) coordinates and (ξ, ζ) coordinates can be derived with reference to figure 1. In figure 1a Δ^s SMN and SO′N′ are similar, from which

$$x = D\xi/(1-\xi\sin\phi) \tag{1}$$

and pyramids SPMN and SP′N′O′ are similar, from which

$$y = D\zeta/(1-\xi\sin\phi) \tag{2}$$

where

$$\sin\phi = (\zeta^2+\xi^2)/2\xi. \tag{3}$$

Equations (1) and (2) are not linear, which result in the distortion of the recorded

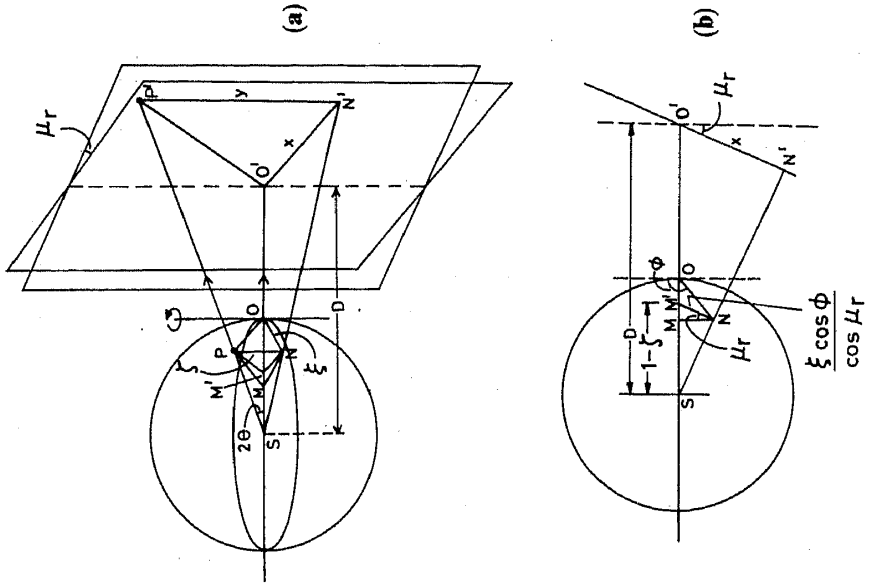

Figure 2. Rotation axis normal to the x-ray beam and film tilted about the rotation axis by μ_r. (**a**) Perspective view. (**b**) Projection perpendicular to the rotation axis.

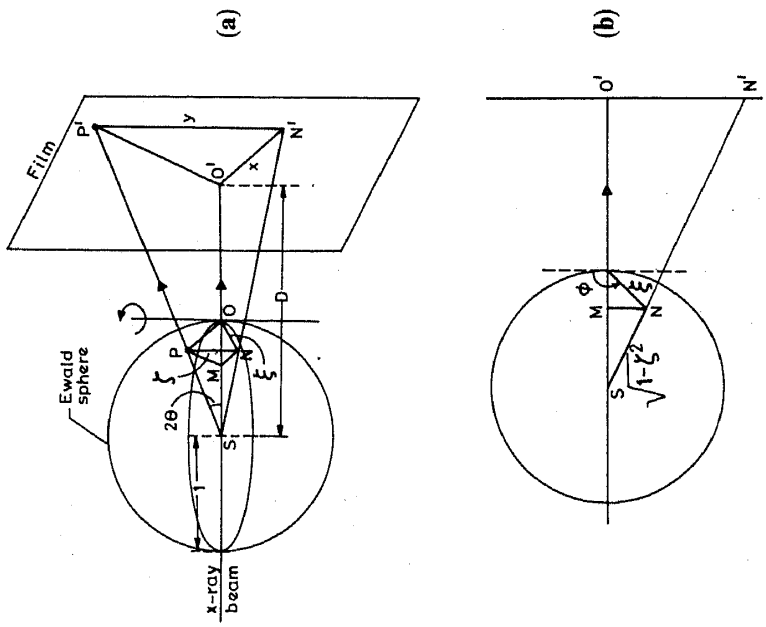

Figure 1. Rotation axis and film normal to the x-ray beam. (**a**) Perspective view. (**b**) Projection perpendicular to the rotation axis.

RL. Also, from equation (3) it follows that for a given ζ the RL points smaller than $\xi=1-(1-\zeta^2)^{1/2}$ are not recorded.

5. Film tilted by μ_r about the rotation axis

The distortion of the recorded image may be eliminated by tilting the film about the rotation axis. When the film is tilted to make it parallel to a (ξ, ζ) plane, the corresponding RL point is projected on the film without distortion. The film can be brought parallel to many (ξ, ζ) planes by tilting it continuously between $-\mu_0$ and $+\mu_0$. However, reflections from other planes are recorded in a distorted way.

This situation, when the film is tilted by μ_r about the rotation axis, is illustrated in figure 2.

From similar $\triangle^s$ SM′N and SO′N′, it can be shown that

$$x=\frac{D\xi\cos\phi}{\cos\mu_r[1-\xi(\sin\phi-\cos\phi\cdot\tan\mu_r)]} \tag{4}$$

and from similar pyramids SM′PN and SO′P′N′,

$$y=\frac{D\zeta}{1-\xi(\sin\phi-\cos\phi\tan\mu_r)}. \tag{5}$$

When μ_r varies between $-\mu_0$ and $+\mu_0$ the image of an RL point is a curve described by equations (4) and (5). When $\mu_r=\phi$, ($x=D\xi$ and $y=D\zeta$) the reflection is recorded without distortion, which also lies on the curve.

6. Crystal and film tilted by μ_t with respect to the x-ray beam

The RL points which are unrecorded in the rotation photograph can be recorded by tilting the crystal and the film with respect to the beam. When the crystal is tilted, the RL point which has been just touching the Ewald sphere will either go in or come out of the sphere depending upon the tilt. However, it will come to the surface of the sphere again at new ϕ. This is depicted in figure 3, where the crystal and the film are shown tilted by μ_t. The expression for ϕ in terms of μ_t is given by,

$$\sin\phi=(\zeta^2+\xi^2-2\zeta\sin\mu_t)/(2\xi\cos\mu_t). \tag{6}$$

This shows that, for a given ζ, the minimum value of ξ that can be recorded decreases as μ_t increases. So, the RL points on the rotation axis and those closer to it can be recorded by tilting the crystal. In figure 3, $\triangle^s$ SMN and SQ′N′ are similar and hence

$$x=(D\xi\cos\phi\cos\mu_t)/(\cos\mu_t-\xi\sin\phi) \tag{7}$$

and pyramids SMNP and SQN′P′ are similar and hence,

$$y=\frac{D[\zeta\cos\mu_t-\xi\sin\mu_t\sin\phi]}{\cos\mu_t-\xi\sin\phi}. \tag{8}$$

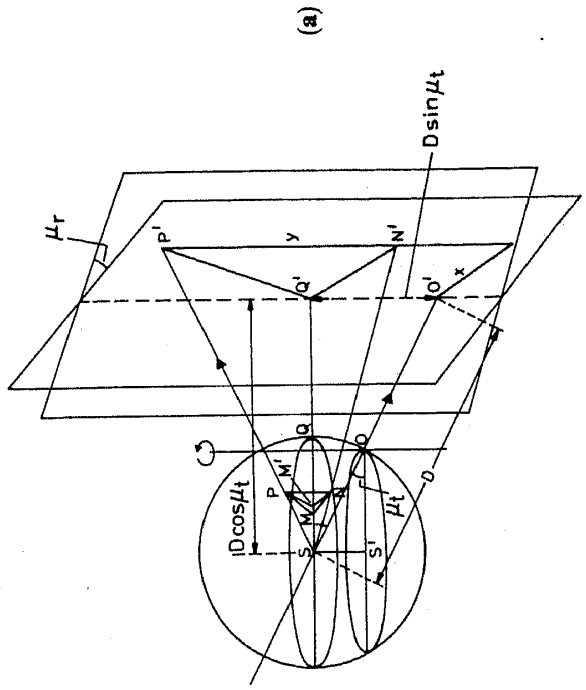

Figure 4. Rotation axis and film tilted by μ_t with respect to the x-ray beam and film tilted by μ_r about the rotation axis. **(a)** Perspective view. **(b)** Projection perpendicular to the rotation axis.

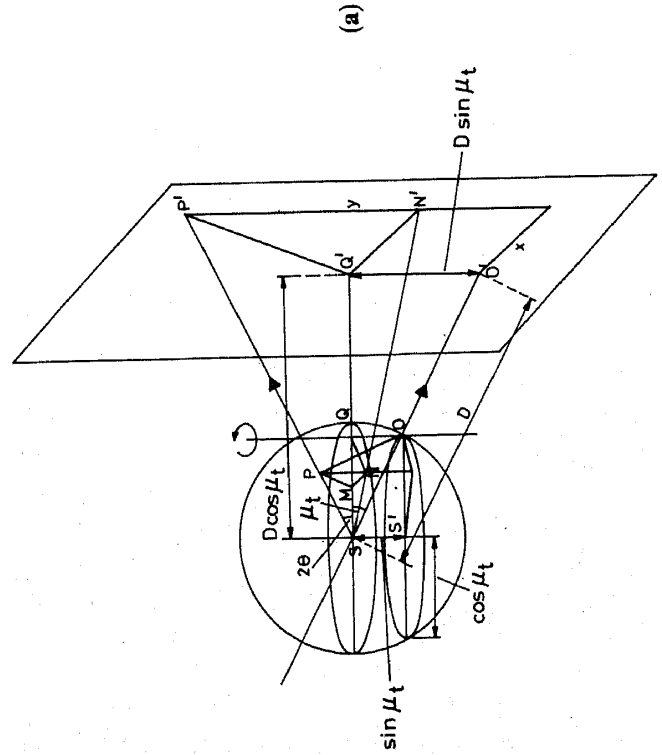

Figure 3. Rotation axis and film tilted with respect to the x-ray beam by μ_t. **(a)** Perspective view. **(b)** Projection perpendicular to the rotation axis.

When μ_t varies between $-\mu_0$ and $+\mu_0$ the image of an RL is recorded in a curve according to (7) and (8), which, when $\mu_t = 0$, reduce to equations (1) and (2) respectively, corresponding to the rotation photography.

7. Crystal and film tilted by μ_t with respect to the x-ray beam and film tilted by μ_r about the rotation axis

Combination of the last two cases simultaneously eliminates the two disadvantages of the rotation photograph. This situation is depicted in figure 4, with the crystal and the film tilted by μ_t with respect to the beam and the film tilted by μ_r about the rotation axis.

From similar $\triangle^s$ SM'N and SQ'N',

$$x = \frac{D\xi \cos\phi \cos\mu_t}{\cos\mu_r[\cos\mu_t - \xi(\sin\phi - \cos\phi \tan\mu_r)]} \tag{9}$$

and from similar pyramids SM'PN and SQ'P'N',

$$y = \frac{D[\zeta \cos\mu_t - \xi \sin\mu_t(\sin\phi - \cos\phi \tan\mu_r)]}{[\cos\mu_t - \xi(\sin\phi - \cos\phi \tan\mu_r)]}. \tag{10}$$

When $\mu_r = \phi$, these expressions reduce to

$$x = D\xi \quad \text{and} \quad y = D\zeta. \tag{11a, b}$$

The optimum value of μ_r for an RL point to be recorded without distortion depends on ϕ, which in turn depends on μ_t. This condition can be satisfied for all RL points by varying both μ_r and μ_t simultaneously with the help of the Buerger precession camera, which is discussed in the next section.

8. Rotation-precession photography

In a precession camera, the orientation of the film during its precession can be decomposed into two tilt components, $\mu_r = \mu_0 \cos\theta$ and $\mu_t = \mu_0 \sin\theta$, where μ_0 is the precession setting angle. Both μ_r and μ_t vary, with μ_r being maximum when μ_t is 0 and vice versa. This makes it possible to bring the film to required orientations for different RL points to be recorded without distortion. However, each RL point will be contributing to its image during the full cycle of precession. So each RL point is imaged into a closed curve on the film according to (9) and (10).

Rotation of the crystal, during the precession, brings each RL point on the "zero plane" at one moment, at which it produces a single image in the correct place and during all other times, the point lies out of the plane giving double images. When it does not lie on the zero plane, it can be considered as lying on higher planes. When a zero layer screen is used these higher plane image points are cut off and only zero plane image points are recorded. The resulting photograph is an overlapped-undistorted photograph of all zero planes. These aspects are discussed by King (1966) in detail.

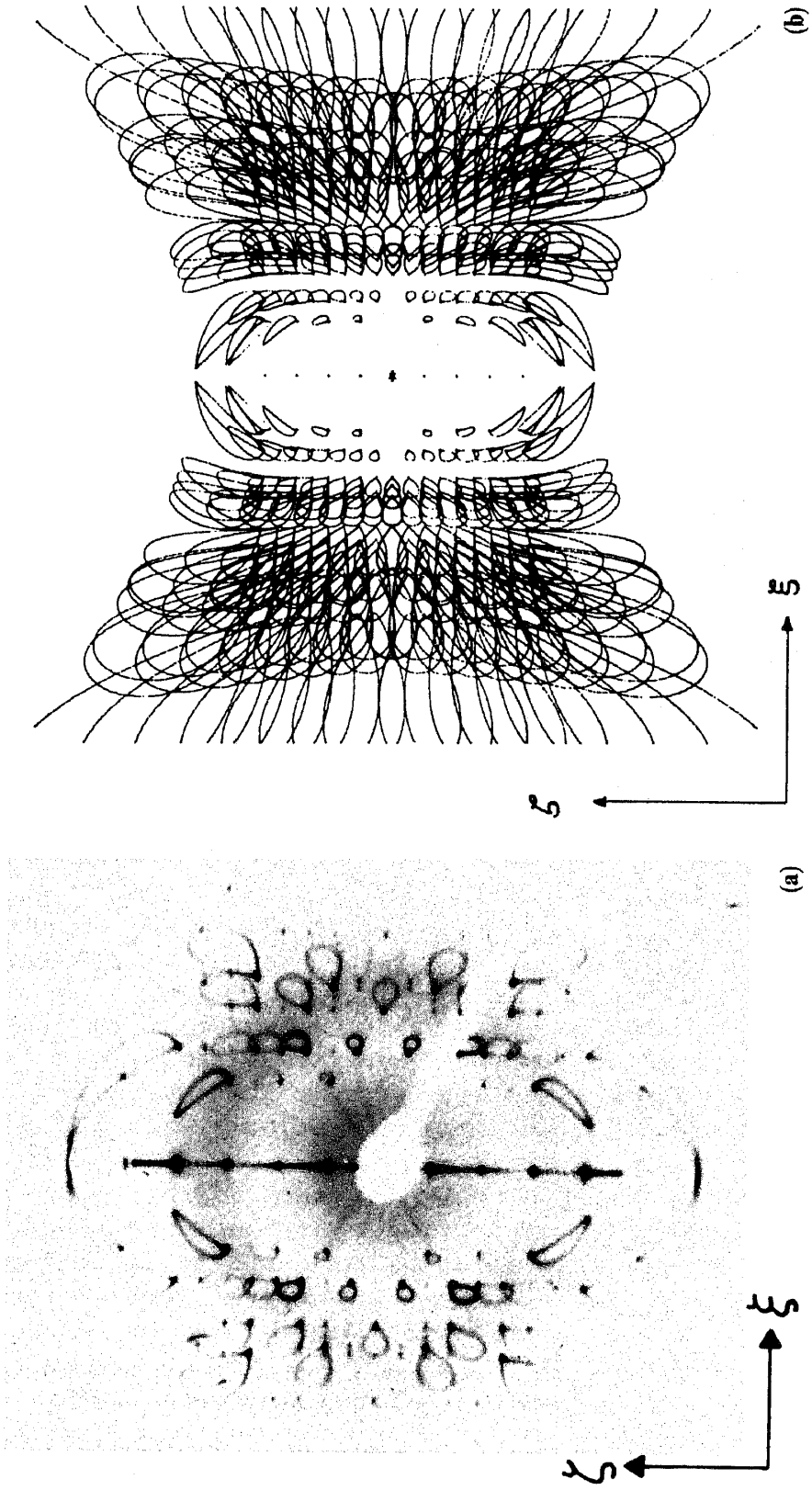

Figure 5. Screenless rotation-precession pattern of crystal of glycyl-DL-phenylalanine (CuK_α, $\lambda = 1{\cdot}5418$ Å; crystal to film distance = 60·0 mm). (**a**) Experimental (**b**) Calculated.

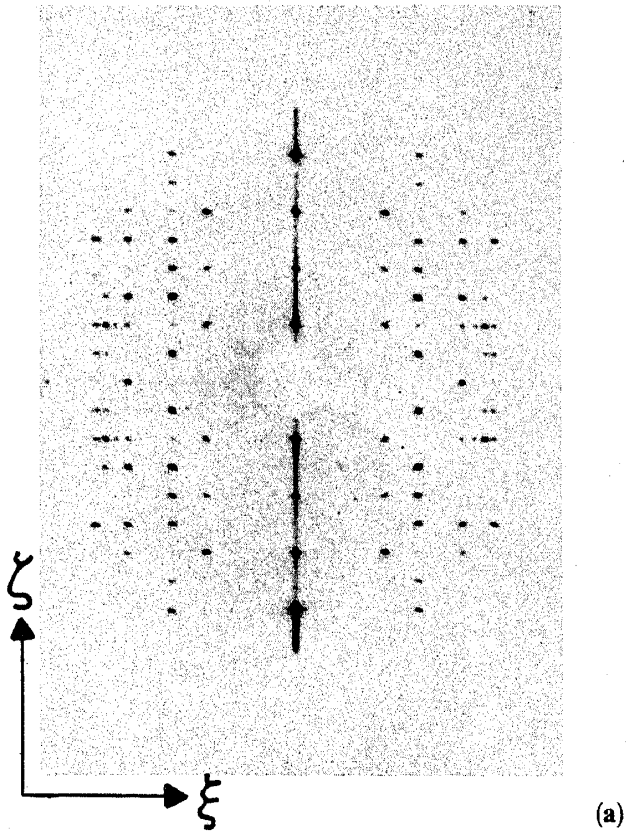

(a)

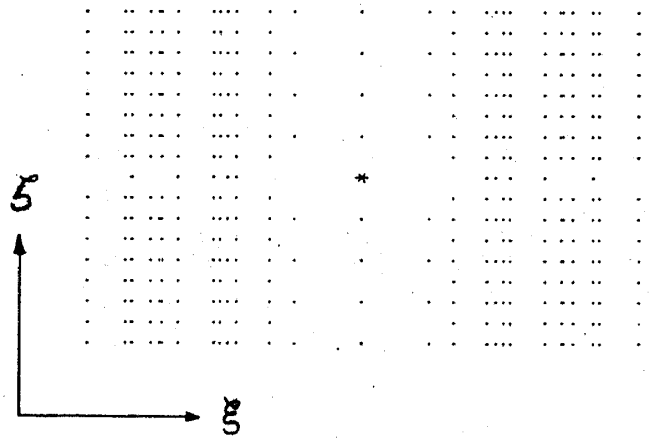

(b)

Figure 6. Screened rotation-precession pattern (CuK_α, $\lambda = 1{\cdot}5418$ Å; crystal to film distance = 60·0 mm; zero level screen radius = 10·0 mm). **(a)** Experimental. **(b)** Calculated.

9. Experimental verification

The theory presented in this paper has been tested with experiments on a crystal of glycyl-DL-phenylalanine (Space Group: P_{bca}; $a=9{\cdot}241(2)$ Å, $b=28{\cdot}91(2)$ Å and $c=8{\cdot}602(2)$ Å.) (Marsh *et al* 1976). The crystal has been mounted on the precession camera (make: Huber, D 8211 Rimsting, Germany) with the crystal to film distance of 60 mm. It has been well aligned to the accuracy of 0·1° on both the arcs to ensure that there is no splitting of reflections due to the misalignment of the crystal. The precession motion of the film has been coupled with the oscillation motion of the crystal in the plane containing the x-ray beam and the spindle axis. In addition, the crystal has been rotated continuously about the spindle axis. The crystal has been exposed with CuK_α radiation ($\lambda=1{\cdot}5418$ Å) filtered with Ni filter.

Figure 5a shows the screenless rotation-precession photograph of the crystal rotated about b-axis with 15° precession. Figure 5b shows the simulated rotation-precession pattern using (9) and (10). Figure 6a shows the screened rotation-precession photograph of the crystal and figure 6b is the calculated pattern with the condition

$$\mu_r=\sin^{-1}\left[\frac{\zeta^2+\xi^2-2\zeta\sin\mu_t}{2\xi\cos\mu_t}\right]. \tag{12}$$

The similarity of experimentally recorded photographs and analytically constructed patterns, both with and without screen, confirms the correctness of the expressions.

Systematic absences of the space group have been avoided in the simulated patterns. Although the geometry of the reflections is identical in both experimental and calculated patterns, the intensities of the reflections unavoidably differ. The intensities of the reflections in the experimental patterns depend on the nature of the atoms present in the unit cell. This variation was not incorporated in the calculations.

10. Conclusions

The reflections in the screened 'rotation-precession' photograph are distributed in equally-spaced straight layers, making the measurements and calculations easier, which, otherwise, would be distributed in unevenly spaced hyperbolic layers in a rotation photograph (Buerger 1966). Also, it contains reflections corresponding to small ξ values including those observed in the rotation photograph. These features have been observed in the photographs of DNA fibres also. For example, meridional reflections have been observed on the fourth and sixth layers of the precession photograph of B-DNA fibre, which are missing in the flat plate photograph. The application of the precession method for the DNA fibres and finer details obtained from the photographs are discussed in detail by Sundaramoorthy *et al* (1986).

Acknowledgements

The author thanks Prof. V Sasisekharan for his guidance and encouragement, Dr M R N Murthy for valuable discussions and Mr N Srinivasan for his help in

computer plotting. The author also thanks the Department of Science and Technology (India) for a fellowship.

References

Buerger M J 1964 *The precession method in x-ray crystallography* (New York: John Wiley)
Buerger M J 1966 *X-ray crystallography* (New York: John Wiley) p. 93
Howsman J A and Walter N M 1960 *Physical methods in chemical analysis* (ed.) W G Berl (New York: Academic Press) Vol. 1, p. 129
King M V 1966 *Acta Crystallogr.* **21** 629
Marsh R E, Ramakumar S and Venkatesan K 1976 *Acta Crystallogr.* **B32** 66
Sundaramoorthy M, Parrack P K and Sasisekharan V 1986 *Biomolecular Stereodynamics* (eds) R H Sarma and M H Sarma (New York: Adenine press) Vol. 4, p. 217

Pramāṇa – J. Phys., Vol. 28, No. 4, April 1987, pp. 415–424. © Printed in India.

Precession photography of fibres: Prediction of patterns

M SUNDARAMOORTHY
Molecular Biophysics Unit, Indian Institute of Science, Bangalore 560 012, India

MS received 21 November 1986; revised 25 February 1987

Abstract. The Buerger precession method of recording x-ray diffraction patterns can also be used for fibres. This method has some advantages over the conventional flat plate method. Since the fibre has inherent cylindrical symmetry, the precession photograph of the fibre is equivalent to the 'rotation-precession' photograph of a single crystal. An analytical prediction of diffraction patterns of the rotation-precession photography is discussed. Also, experimental data are provided to confirm the validity of the equations derived.

Keywords. Fibre; diffraction; precession method; pattern prediction.

PACS No. 61·10

1. Introduction

X-ray diffraction patterns of fibres are generally recorded with flat plate cameras. Occasionally, necessity arises to record the meridional and near meridional reflections in the investigation of fibres. In such instances, fibres are tilted, with respect to the x-ray beam through a particular angle corresponding to the layer of interest. The major disadvantage of this method is that it requires recording of as many photographs as the number of layers and also prior knowledge of the period of repeat along the fibre axis for the calculation of tilt angles. Howsman and Walter (1960) had suggested the application of the well-known Buerger precession method which permits meridional and near-meridional reflections to be recorded on a single photograph. In addition, the precession method results in an undistorted image of the reciprocal lattice (RL). King (1966) analyzed the imaging geometry and related the resolution to the layer line screen parameters and the precession angle. He had developed a graphical method of visualizing the images using the geometrical construction of Buerger (1964). This article presents an analytical approach to constructing diffraction images produced by fibres in the precession geometry. The analysis presented here was developed from an earlier study on the "rotation-precession method" using single crystals (Sundaramoorthy *et al* 1986).

2. Diffraction geometry

The RL of a uniaxial fibre is cylindrically symmetrical about the fibre axis. In other words, the RL of a fibre is made up of rings coaxial with the fibre axis. On the other hand, for a single crystal the RL is made up of discrete points. However, single crystal x-ray diffraction might mimic fibre diffraction on rotating the crystal about a chosen axis. Similarly, precession picture recorded for a fibre is equivalent to a rotation-